Mechanisms to Reduce the Blade Passing Frequency Tone for Subsonic Low-Count OGV Fans

Stephen Schade*, Robert Jaron, Antoine Moreau, Sébastien Guérin

German Aerospace Center (DLR), Müller-Breslau-Straße 8, 10623 Berlin, Germany

Abstract

Conventionally, fan stages are designed with more stator vanes than rotor blades. These fan stages provide a tonal noise advantage as the blade passing frequency tone is cut-off. Contrary to conventional cut-off designs, low-count OGV (Outlet Guide Vane) designs are fan stages with fewer stator vanes than rotor blades. Low-count OGV designs benefit from lower broadband noise due to the reduced number of stator vanes. However, the blade passing frequency tone may no longer be cut-off. Therefore, we assess tonal noise reduction mechanisms for subsonic low-count OGV fan stages. We use an analytical and a numerical method to predict the rotor–stator interaction noise for different blade count pairings. The results indicate that the mode phase propagation angle and the cut-on factor are two acoustic parameters that dominantly influence the noise excitation. For certain blade count pairings an acoustic benefit exists if the mode phase propagation angle is congruent to the stator leading edge angle and / or if the mode is away from the cut-off limit. Moreover, reducing the rotor tip speed allows, for some configurations, a cut-off design even with fewer stator vanes than rotor blades (inverse cut-off). Overall, the study shows promising possibilities to reduce tonal interaction noise for low-count OGV fan stages.

Keywords: Fan noise, low-count OGV fans, design-to-noise, tonal noise reduction, inverse cut-off, urban air mobility

1. Introduction

The noise impact of urban air mobility (UAM) airplanes has attracted increasing attention as these airplanes are expected to take off and land in highly populated areas. Especially for electrically powered airplanes operating in urban areas, fan noise will be a crucial challenge. Current UAM airplane concepts include, in addition to open-rotor variants, airplanes equipped with low-speed shrouded fan stages. These fan stages may be arranged either as a double configuration or as a distributed propulsion system. A significant contribution to the overall noise impact of the aircraft will be caused by the fan stages [1, 2]. Rizzi et al. [3] highlighted the demand to "document noise reduction

*Corresponding author

Email address: stephen.schade@dlr.de (Stephen Schade)

technologies available for UAM" as one "high-level goal" for the development of UAM airplanes. Referring to this demand, we intend to investigate and evaluate noise reduction mechanisms for low-speed shrouded fan stages of small airplanes. Our objective is to provide a step towards the design-to-noise of fan stages.

Conventionally, fan stages are designed with significantly more stator vanes than rotor blades. This approach leads to an advantage regarding tonal interaction noise since the blade passing frequency tone, which is usually dominant, is cut-off. Although cut-off designs have a tonal advantage, these designs are not beneficial regarding broadband noise. The broadband noise source can be efficiently decreased by reducing the stator vane count since this noise source roughly scales with the number of stator vanes [4].

Contrary to a conventional cut-off design, a low-count OGV (Outlet Guide Vane) design is a fan stage with fewer stator vanes than rotor blades. Compared to a cut-off design, a low-count OGV design is more advantageous with regard to manufacturing costs as well as broadband interaction noise. However, the usually dominant blade passing frequency tone may no longer be cut-off due to the reduced number of stator vanes. This may cause a tonal noise penalty. In order to mitigate this tonal disadvantage, we investigate mechanisms that reduce the noise levels of the blade passing frequency tone. Our intention is to outline and understand the acoustic effects that may provide a benefit for low-count OGV designs. As a long-term goal, we ask the research question: Can low-count OGV designs compete with the noise levels of conventional cut-off designs? As a first step towards answering this question, we put an emphasis on the tonal noise excitation and assess three noise reduction mechanisms for subsonic low-count OGV fans: The mode phase propagation angle (1), the mode cut-on factor (2) and the inverse cut-off of the blade passing frequency tone (3).

There are few studies in the literature regarding the acoustic potential of low-count OGV designs. Dittmar et al. [5, 6] examined different low-count OGV fan stages and compared the noise levels to conventional designs. The results indicate that low-count OGV designs benefit from lower broadband noise and a reduced noise annoyance. Schwaller et al. [7] experimentally investigated different rotor–stator blade count pairings and measured the far-field noise. They confirmed that low-count OGV designs have benefits with regard to broadband noise and identified a reduction of the higher harmonic blade passing frequency tones. Thereupon, Kröger et al. [8] conducted a multidisciplinary optimization of a low-count OGV fan stage. Regarding aerodynamics, they concluded that a reduction from 42 to 14 stator vanes is feasible and even suitable. Regarding acoustics, they observed an increase in the first blade passing frequency tone. To address this noise penalty, Giacché et al. [9] performed an acoustic optimization of a low-count OGV fan stage. The optimized OGV had a modified leading edge profile with non-uniform sweep distribution. They showed that the modification decreases the noise levels of the blade passing frequency tone [9]. Recently, Jaron [4] examined low-count OGV designs regarding their potential to reduce tonal noise and identified that certain blade count pairings benefit from a weaker excitation of the dominant modes. The study indicates that the relative angle between the mode phase propagation angle and the stator leading edge angle is a reason for a lower noise excitation [4]. However, the impact of the mode phase propagation angle on the noise excitation is not fully understood yet. Therefore, we further investigate this effect within the present paper.

To examine the tonal noise reduction mechanisms, we perform a variation of the rotor and stator blade count. The idea is to identify promising blade count pairings that lead

to lower noise levels. Casalino et al. [10] described this approach as a "best practice" to decrease "the fan rotor/stator interaction noise". For each blade count pairing we predict the noise levels analytically. For selected blade count pairings we perform Harmonic Balance simulations to validate the analytical prediction. The fan stage for the noise assessment is described in Sec. 2, the analytical fan noise prediction method in Sec. 3 and the numerical method in Sec. 4. The impact of the mode phase propagation angle and the impact of the mode cut-on factor on the noise excitation are assessed in Subsec. 5.1. Afterwards, the relation between the inverse cut-off effect and the rotor tip speed is examined in Subsec. 5.2.

2. Baseline fan stage

For the acoustic analysis, the "Co / Contra Rotating Acoustic Fan Test rig" (CRAFT), operated by the Department of Engine Acoustics of the German Aerospace Center, is used [11]. The CRAFT rig can be equipped either with two counter-rotating rotors or with a co-rotating rotor–stator stage [12]. The latter configuration is shown in Fig 1. For the acoustic predictions, presented in this paper, the rotor–stator stage is scaled by a factor 2 : 1. The reason is that the thrust level provided by the scaled fan stage would be sufficient to power a small twin-engine aircraft. Thus, the CRAFT rig is representative for a shrouded fan stage of a small airplane, which could be operated in an UAM mission. Table 1 summarizes the design and sideline operating points for the scaled CRAFT rotor–stator stage. The latter is used for the subsequent analysis since it is the loudest operating point of the relevant acoustic noise certification points approach, sideline and cutback.

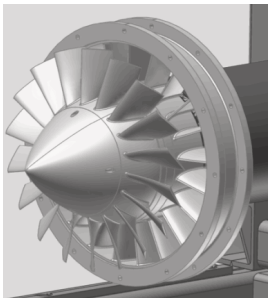

Figure 1: CRAFT rotor–stator configuration.

	Design	Sideline
fan diameter [m]	0.908	
pressure ratio	1.039	1.050
mass flow [kg/s]	22.70	24.11
rotational speed [rpm]	2194	2356
rel. rotor tip Mach number	0.31	0.33

Table 1: Design and sideline operating points for the scaled CRAFT rotor–stator stage.

3. Analytical fan noise prediction method

Different analytical and semi-analytical methods for predicting fan noise exist. Casalino et al. [10] provide a bibliographic overview of such approaches and emphasize that these are essential for the design-to-noise of fan stages. In this paper, the fan noise prediction is performed with the tool "PropNoise" (PN), developed by the Department of Engine Acoustics of the German Aerospace Center [13]. Particularly, the noise levels are calculated with the stand-alone module of PropNoise. The stand-alone module provides an aerodynamic preliminary design of the fan stage and a fully analytical noise

prediction. The input data are the fan geometry (e.g. diameters, blade count numbers, chord lengths) and the design operating conditions as for example mass flow and rotational speed. The steady and unsteady aerodynamics are calculated at a single meanline position, which is considered as representative for the complete flow. The meanline radius is located at 70% blade span. Subsequently, the aerodynamic solution is extrapolated in radial direction. The data generated in the aerodynamic modules constitute the input for the acoustic module, which relies on a radial-strip approach. That means, the module determines the response of the blade to an aerodynamic excitation for each radial strip as if the problem was two-dimensional. Afterwards, the source term is integrated in radial direction in order to determine the sound pressure amplitude and the sound power propagating within the duct segments [13].

The subsequent acoustic analysis relies on the evaluation of the phase propagation angle ζ_{mn} and the cut-on factor α_{mn} of an acoustic mode of azimuthal and radial order (m, n). In the ray tracing theory, the phase propagation angle describes the propagation of an acoustic ray in a duct. According to [14, 15], in absence of swirl, ζ_{mn} is defined as

$$\zeta_{mn}^{\pm} = -\text{sign}\,(m) \cos^{-1}\left(\frac{-M_x \pm \alpha_{mn}}{1 \mp \alpha_{mn} M_x}\right). \tag{1}$$

In Eq. (1) the superscript $\pm$ indicates the direction of propagation, where $+$ is used for the downstream direction and $-$ for the upstream direction. The phase propagation angle depends on the sign of the azimuthal mode order m, the axial Mach number M_x and the mode cut-on factor α_{mn}. As described in [13, 16] and under consideration of a solid body swirl, this factor is given by

$$\alpha_{mn} = \sqrt{1 - (1 - M_x^2)\left(\frac{\sigma_{mn}}{kR - mM_s}\right)^2}. \tag{2}$$

In Eq. (2) the variable σ_{mn} is the $(n+1)^{th}$ zero of the first derivative of the radial eigenfunction at the walls, k is the acoustic wave number, R is the duct radius and M_s is the swirl Mach number. At the stator entry, the duct radius is $R = 0.454\,\text{m}$, the swirl Mach number is $M_s = 0.13$ and the axial Mach number is $M_x = 0.15$. Note that Eq. (1) is only valid for piecewise linear rays. Under consideration of flow swirl, the rays would be curved. Flow swirl is only considered for the calculation of the cut-on factor, as indicated in Eq. (2).

The cut-on factor is a criterion to determine the propagation capability of acoustic modes within a duct [13]. For propagating modes, α_{mn} is a real number and ranges between 0 and 1. Towards the limit of 0, the modes still propagate, but are close to cut-off and for well-propagating modes, α_{mn} tends towards 1. For non-propagating modes (cut-off modes), α_{mn} has an imaginary part which leads to the exponential decay of the acoustic pressure [13, 16].

Based on the acoustic pressure of an azimuthal mode m and the in-duct Green's function $\hat{g}_{mn}^{\omega}$ an expression for the modal pressure amplitude can be formulated. According to the derivation which is presented in [13, 16], the modal amplitude for the in-duct case and Tyler–Sofrin modes is formulated as

$$A_{mn}^{\pm} = i \cdot B \int_r^R \hat{g}_{mn}^{\omega}\; e^{-ik_x x_{LE} - im\theta_{LE}} \cdot \sigma \cdot dr_s. \tag{3}$$

In Eq. (3), B is the number of rotor blades, r is the duct radius at the hub, R is the duct radius at the tip, k_x is the axial wavenumber and x_{LE} and θ_{LE} are the axial and circumferential leading edge positions. The in-duct Green's function $\hat{g}^{\omega}_{mn}$ is given by

$$\hat{g}^{\omega}_{mn} = \frac{i}{4\pi R} \cdot \frac{J_m(k_r r_s) + Q_{mn} Y_m(k_r r_s)}{kR\ \alpha_{mn}\sqrt{F_{mn}}}, \tag{4}$$

where J_m are the Bessel functions, Y_m are the Neumann functions, k_r is the radial wavenumber, r_s is the radial coordinate at the source position, F_{mn} are normalization factors and the quantity Q_{mn} is equal to zero for hollow ducts [13, 17].
In Eq. (3), the quantity σ includes several source terms, i.a. a term for the lift noise component σ_L. This term is given by

$$\sigma_L = i\, k_n \int_0^c f_L^{\hat{\omega}} \cdot e^{-ik_l l} dl, \tag{5}$$

where $f_L^{\hat{\omega}}$ is the chordwise distribution of lift, k_l is the chordwise wavenumber and l is the chordwise position of the noise source on the blades [16]. From Eq. (5) it can be obtained that the lift-generated tonal noise component is affected by the normal wavenumber k_n [13]:

$$k_n = (k - \frac{mM_s}{R})\ \sin(\zeta^{\pm}_{mn} - \chi_{LE}) \tag{6}$$

According to Eq. (6), the relation between the mode phase propagation angle $\zeta^{\pm}_{mn}$ and the stator leading edge angle χ_{LE} influences the normal wavenumber and thus affects the source term σ_L for the lift noise component and its modal amplitude $A^{\pm}_{mn}$.
Following the derivation presented in [16, 18], the acoustic modal power under consideration of a solid body swirl is determined from

$$P^{\pm}_{mn} = \frac{1}{1 - \frac{mM_s}{kR}}\ \pi R^2\ \frac{\alpha_{mn}}{\rho_0\, a_0}\ \frac{(1 - M_x^2)^2}{(1 \mp \alpha_{mn} Mx)^2}\ |A^{\pm}_{mn}|^2, \tag{7}$$

where ρ_0 is the static density and a_0 is the speed of sound. In the following, the tonal sound power levels at noise generation, i.e. at the stator leading edge, are analyzed.
The tonal wake interaction noise can be classified as unsteady lift-generated noise. The driving physical mechanism for this noise source is a time-dependent variation of the pressure distribution on the blade surface. The pressure variation is caused by the rotor wake which impinges on the stator leading edge. A dipole noise source results from this interaction between the blade profile and the incoming flow, as schematically illustrated in Fig. 2. Hence, the tonal wake interaction noise can be represented by dipoles located at the stator leading edge [19].
In PropNoise, the blade profiles are modeled as infinite thin flat plates which are staggered at an angle χ relative to the engine axis, where χ_{LE} is the stator stagger angle at the leading edge (see Fig. 2). The main radiation axis of the dipole source is perpendicular to χ_{LE} at the source position. In the subsequent analysis, the mode phase propagation angle ζ_{mn} will be put in relation to the stator stagger angle at the leading edge χ_{LE} in order to evaluate the impact of these quantities on the noise generation. Note that ζ_{mn} and χ_{LE} are defined positive in $-\theta$ direction. In reality, typically twisted stator vanes are used which means that the leading edge angle radially changes. This is considered for

the numerical simulations. However, for the analytical noise prediction, untwisted stator vanes are used. Thus, the leading edge angle is treated as constant in radial direction and the approach illustrated in Fig. 2 is valid.

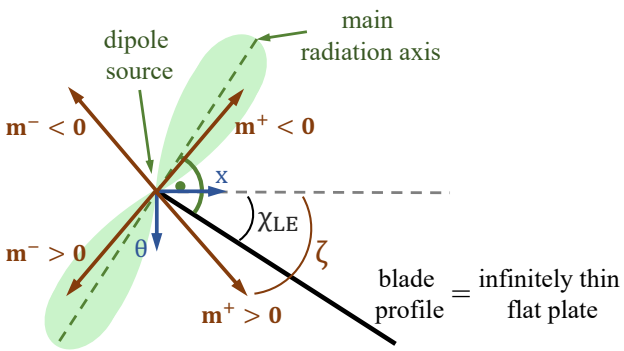

Figure 2: Relation between mode propagation angle and noise generation at the stator leading edge.

The difference between the stator leading edge angle and the mode phase propagation angle is denoted with Δ and for the subsequent analysis Δ is scaled to the range $[0, 90\,\text{deg}]$. Accordingly, Δ can be determined from

$$\Delta = \begin{cases} |\zeta_{mn} - \chi_{LE}|, & \text{if } |\zeta_{mn} - \chi_{LE}| \leq 90\,\text{deg} \\ |180 - |\zeta_{mn} - \chi_{LE}||, & \text{if } |\zeta_{mn} - \chi_{LE}| > 90\,\text{deg} \end{cases} . \tag{8}$$

As seen in Eq. (3), Eq. (5) and Eq. (6), if the mode phase propagation angle is exactly congruent to the stator leading edge angle, the acoustic mode will not be excited ($\Delta = 0\,\text{deg}$, $\zeta_{mn} = \chi_{LE}$). In that particular case, the phase propagation angle of the acoustic mode is perpendicular to the dipole radiation axis. On the contrary, if the mode phase propagation angle is in line with the dipole radiation axis, the strongest sound excitation occurs. In that particular case, the phase propagation angle of the acoustic mode is perpendicular to the stator leading edge angle ($\Delta = 90\,\text{deg}$).
Further, Fig. 2 exemplarily shows the propagation directions of upstream ($-$) as well as downstream ($+$) propagating positive and negative azimuthal acoustic modes m. For instance, $m^+ > 0$ is a positive and downstream propagating acoustic azimuthal mode. The sign convention of the azimuthal modes can be determined by applying the curl right hand rule in the direction of the x-axis.

4. Numerical fan noise prediction method

A numerical fan noise prediction is performed for selected rotor–stator combinations. The in-house Navier-Stokes solver "TRACE" [20, 21], specifically developed for turbomachinery applications, is applied to numerically predict the unsteady flow field. We use TRACE to perform Harmonic Balance simulations (HB simulations). The HB method applies a Fourier transformation of the Reynolds Averaged Navier Stokes equations (RANS equations) and solves them in the frequency domain for selected frequencies, which are non-linearly coupled [22–24]. The closure of the RANS equation system is achieved with the Menter SST $k - \omega$ turbulence model [25]. For both the rotor blade row and the stator vane row one flow passage with phase-shifted boundary conditions

in circumferential direction is modeled. As a consequence, the simulation results only include those flow effects that are circumferentially periodic with the number of rotor blades and stator vanes.
The structured grid has an O-C-H topology around the blades. In spanwise direction, the grid consists of 90 cells, of which 9 cells are placed in the rotor tip gap. In circumferential direction, the grid resolves the smallest considered acoustic wave length with more than 35 cells per wave length. On the airfoil surfaces, the size of the first grid cell resolves the laminar sublayer of the velocity boundary layer ($y^+ < 1$). In total, the computational grid of the rotor–stator stage consists of more than $17 \cdot 10^6$ cells.
Several criteria are used to evaluate the convergence. For instance, the mass flow and pressure are monitored at the inlet and outlet of the computational domain to assess the behavior of these flow quantities as the solution evolves. For the HB simulation an additional acoustic convergence criterion is specified: Monitor plots trace the sound power levels (PWL) of the propagating modes of the first and second blade passing frequencies (BPF1, BPF2). For the converged solution the sound power levels have reached a constant value and the residuals are smaller than 10^{-5}. Compared to the initial solution the residuals have dropped by at least three orders of magnitude.
An extended triple plane pressure mode matching (XTPP) method is applied to extract the acoustics from the simulation [26]. The XTPP approach is based on the method originally developed by Ovenden and Rienstra [27]. The extension of the method enables to better distinguish between convective and acoustic perturbations and leads to an improved prediction of tonal noise [26].

5. Results

Based on the scaled CRAFT geometry, a variation of the rotor and stator blade count is performed using the stand-alone module of PropNoise. The CRAFT rig has 18 rotor blades and 21 stator vanes. This is the initial configuration for the blade count variation. The variation is carried out at constant solidity to achieve a similar aerodynamic blade loading. Thus, the chord length changes between the configurations. For instance, the lower the number of rotor blades or stator vanes the longer the blade or vane chord. The initial configuration is used to determine the chord lengths of all other blade count pairings based on the condition that the solidity is constant. Further, the distance between the rotor trailing edge and stator leading edge remains constant. Hence, the propagation distance of the rotor wake up to the stator leading edge is identical for all configurations.
Figure 3 shows the analytically predicted sound power levels of the BPF1 tone for different rotor–stator blade count pairings. All low-count OGV configurations are framed in green and the dotted yellow line shows the BPF1 cut-off border. Within the low-count OGV design space, we identified three subareas with lower overall BPF1 sound power levels. We named these subareas “A”, “B” and “C”. In Subsec. 5.1 we analyze the acoustic effects that cause blade count pairings in areas “A” and “B” to have lower sound power levels than adjacent blade count pairings. In Subsec. 5.2 we put the focus on the configurations from area “C”.

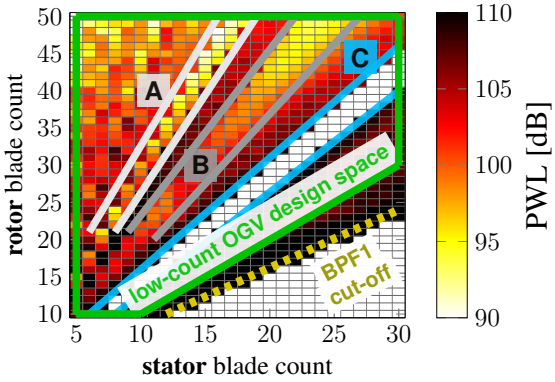

Figure 3: BPF1 sound power level for different rotor–stator blade count combinations.

5.1. Phase propagation angle and cut-on factor

The studies by Guérin et al. [28] and Jaron [4] indicate that the sound power decreases if the phase propagation angle of an acoustic mode is congruent to the stator leading edge angle. To better understand this effect, we examine selected configurations from area "A" in more detail. For this purpose, the number of rotor blades is kept constant and set to $B = 35$. This ensures that the width and depth of the rotor wakes remain identical. The number of stator vanes varies between $V = 11$ and $V = 14$. The configurations with $V = 12$ and $V = 13$ stator vanes belong to area "A". For equidistant blades, the triggered azimuthal mode orders m are a function of the rotor blade count B and stator vane count V: $m = hB - kV$, where $h \in \mathbb{N}_0$ and $k \in \mathbb{Z}$ (Tyler and Sofrin's rule [29]). For each azimuthal mode order m several radial mode orders n may be cut-on. Each mode has a different propagation direction and thus a different phase propagation angle. Therefore, the angle Δ between the stator leading edge angle and the mode phase propagation angle changes. This leads to a weaker or stronger noise excitation of the acoustic modes.

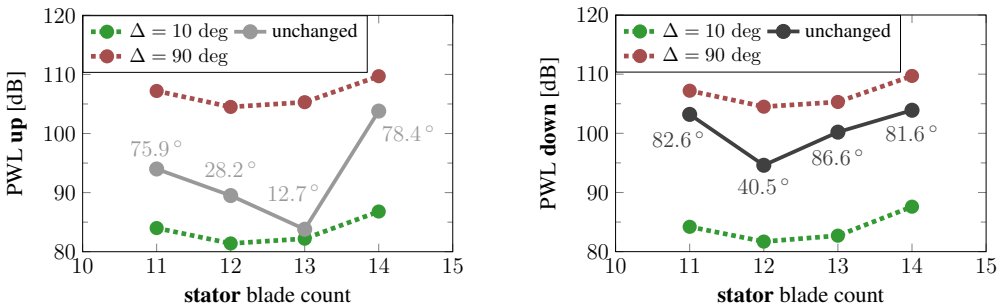

(a) upstream (b) downstream

Figure 4: Upstream and downstream sound power levels of the BPF1 for $B = 35$ and different stator vane counts with unchanged, nearly congruent and perpendicular phase propagation angle relative to the stator leading edge angle. For the unchanged case the inscribed labels indicate the values of Δ for the dominant mode.

Figure 4 depicts the analytically predicted upstream and downstream sound power levels of the BPF1 tone. The labels show the values of Δ for the dominant acoustic

mode of each configuration. The dominant propagating BPF1 modes are summarized in Tab. 2. For a specific acoustic mode, Δ does not change in radial direction, since $\chi_{LE} = -33\,\text{deg} = \text{const.}$ is used for the analytical study. An advantage of the analytical noise prediction is that particular acoustic effects can be examined individually. To specifically assess the impact of the mode phase propagation angle on the noise excitation, we manually manipulated Δ in the PropNoise code. We consider two cases in Fig. 4: 1) A phase propagation angle approximately congruent to the stator leading edge angle ($\Delta = 10\,\text{deg}$) and 2) a phase propagation angle perpendicular to the leading edge angle ($\Delta = 90\,\text{deg}$). In both cases the phase propagation angle is adjusted for all propagating modes. The reason why $\Delta = 10\,\text{deg}$ is applied is that the acoustic modes would not be excited at all if the phase propagation angles were exactly identical with the stator leading edge angle. The dotted green line shows the BPF1 sound power levels for $\Delta = 10\,\text{deg}$. The dotted red line shows the sound power levels for $\Delta = 90\,\text{deg}$. For the latter case the phase propagation angle is in line with the dipole radiation axis. The maximum sound excitation occurs in the direction of the dipole radiation axis. Consequently, it is reasonable that the highest sound power levels are obtained for $\Delta = 90\,\text{deg}$. According to the analytical prediction, the difference of the sound power levels between $\Delta = 90\,\text{deg}$ and $\Delta = 10\,\text{deg}$ is larger than 20 dB. In other words, the manipulation of Δ indicates that for one configuration the sound power level could be more than 20 dB lower, if the phase propagation angles of the propagating modes would be congruent to the stator leading edge angle rather than perpendicular. Thus, the phase propagation angle relative to the stator leading edge has a significant impact on the sound excitation. In particular, the study confirms that acoustic modes having a phase propagation angle congruent to the stator leading edge angle are excited weakly. The results with the actual mode propagation angles, without imposing a fixed value for Δ in the analytical model artificially, are in between the results for $\Delta = 10\,\text{deg}$ and $\Delta = 90\,\text{deg}$.

	upstream				**downstream**			
	(m,n)	α_{mn}	σ_{mn}	Δ [deg]	(m,n)	α_{mn}	σ_{mn}	Δ [deg]
V11	$(2,1)$	0.66	8.55	75.9	$(-9,0)$	0.56	10.65	82.6
V12	$(-1,0)$	0.994	1.25	28.2	$(-1,0)$	0.994	1.25	40.5
V13	$(-4,0)$	0.914	4.95	12.7	$(-4,1)$	0.603	9.71	86.6
V14	$(7,0)$	0.62	8.43	78.4	$(-7,0)$	0.741	8.43	81.6

Table 2: Dominant propagating BPF1 modes for $B = 35$ and varying stator vane count and respective values for α_{mn}, σ_{mn} and Δ.

The effect may be slightly overestimated in the analytical prediction from PropNoise since the stand-alone module uses flat plates to model the blade profiles [4, 13]. In addition, the analytical study is performed with untwisted stator vanes, i.e. the leading edge angle is constant in radial direction. Consequently, for one particular acoustic mode, the difference between the mode phase propagation angle and the stator leading edge angle is also constant. Therefore, we perform a validation of the analytical results using Harmonic Balance simulations. Contrary to the stand-alone module, the HB simulation uses three-dimensional curved blade profiles. Thus, in the HB simulation the leading edge angle radially changes and the dipole sources are distributed along the curved surface. Figure 5 compares the noise prediction from PropNoise with the numerical results obtained from the HB simulation. The numerical data have a constant offset compared to the prediction from PropNoise. However, the numerical results confirm the analytically

predicted trend and verify that also in the numerical simulation the phase propagation angle significantly affects the sound excitation, even though twisted stator vanes are considered.

Besides the stand-alone module, PropNoise offers the option to perform an analytical noise prediction based on RANS simulations [4]. For the RANS-informed analytical noise prediction with PropNoise, all input parameters needed for the acoustics module are extracted from a steady-state RANS simulation. The RANS simulation uses the same fan geometry and blade profiles as the HB simulation. In Fig. 5 the results obtained from the RANS-informed noise prediction are plotted in yellow. These results also confirm the trend predicted by the stand-alone module and exemplarily verify that the assumption of flat plates leads to a reasonable noise prediction.

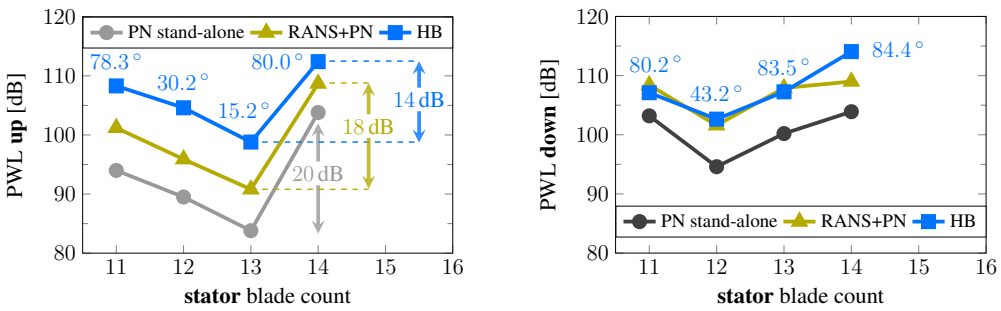

(a) upstream (b) downstream

Figure 5: Upstream and downstream sound power levels of the BPF1 for $B = 35$ and different stator vane counts. Labels indicate the values of Δ for the dominant modes.

The labels inserted in Fig. 5 show the values of Δ. These values are calculated at 70% span. Comparing Fig. 4 with Fig. 5 indicates that the numerically calculated Δ is in good agreement with the analytically predicted value. Regarding the upstream direction, the phase propagation angle is almost congruent to the stator leading edge angle for the configurations B35V12 and B35V13. Note that B35 indicates the number of rotor blades and V13 the number of stator vanes. With regard to B35V13, the dominant Tyler-Sofrin mode is $m = 35 - 3 \cdot 13 = -4$. For this azimuthal mode the phase propagation angle is almost congruent to the stator leading edge angle. Hence, the lowest difference Δ occurs ($\Delta \approx 15\,\text{deg}$). Due to the impact of the phase propagation angle the dominant mode $m = -4$ is excited weakly, which is one reason why B35V13 has the lowest upstream sound power level. Regarding the downstream direction, the phase propagation angle tends to be oriented almost perpendicularly to the leading edge. The only exception is the configuration B35V12. For this configuration PropNoise and the HB simulation predict $\Delta \approx 40\,\text{deg}$, which is the reason for the lower downstream sound power level compared to the adjacent configurations. In addition, PropNoise and the HB simulation predict $\Delta \approx 30\,\text{deg}$ for this configuration in the upstream direction. Thus, the configuration with 12 stator vanes provides a good compromise with regard to the phase propagation angle. This is the first reason why the upstream and downstream BPF1 sound power levels of this configuration are comparable or lower than the sound power levels of adjacent blade count pairings.

For all other blade count pairings from area “A”, we observe a similar result to that

shown in Fig. 4 and Fig. 5. Our interim conclusion for area "A" is that the phase propagation angle of modes propagating upstream is almost congruent to the stator leading edge angle. These modes are excited weakly resulting in a significant tonal noise reduction.

In area "A", the phase propagation angle particularly impacts the sound power levels of the upstream direction. As an additional effect, the mode cut-on factor α_{mn} is identified to influence the sound power levels of the upstream and the downstream direction. The mode cut-on factor provides the explanation why the overall sound power levels are lower in area "A" compared to adjacent blade count pairings. The importance of α_{mn} for modes propagating in ducts was introduced by Rice [30], who identified this factor as a basic parameter for noise propagation. In the following, we investigate the impact of the cut-on factor on the noise generation.

Figure 6 plots the relation between the sound power level and the cut-on factor for the dominant mode. The cut-on factor might be different for the upstream and the downstream direction since different azimuthal and radial modes may be dominant and each set of modes has a different α_{mn}. The cut-on factor is calculated using Eq. (2). The data points colored in red show the analytical prediction for the case that the influence of the phase propagation angle is neglected. That means, Δ is again manipulated in the PropNoise code and set to $\Delta = 90\,\text{deg}$. The results indicate that acoustic modes, which are further away from the cut-off limit ($\alpha \to 1$), are excited weakly and carry a lower sound power. Close to the cut-off limit ($\alpha \to 0$), the sound power increases remarkably, which is also shown in [31]. According to the distribution of the red data points, the relation $\text{PWL} \sim -10\log_{10}(\alpha_{mn}) + y_0$ describes the impact of the cut-on factor on the sound power level. This correlation is deduced from the analytical modeling, which predicts that the sound power is inversely proportional to α_{mn} (see Eq. (3), Eq. (4) and Eq. (7)).

The data points colored in light and dark grey show the actual results from PropNoise without the manipulation of the phase propagation angle. These data points exhibit a larger scattering due to the impact of the phase propagation angle. For instance, for the configuration B35V12 the upstream and downstream phase propagation angles of the dominant Tyler-Sofrin mode $m = -1$ are almost congruent to the stator leading edge angle. Therefore, the data point shifts to a lower sound power level while the cut-on factor remains unchanged. The mode $m = -1$ is excited weakly due to the phase propagation angle. By contrast, if $\Delta = 90\,\text{deg}$ is applied, the mode phase propagation angle is perpendicular to the leading edge angle. As a result, the sound power level increases and the data point is located close to the red curve. For B35V14 both results, with and without the manipulation of the phase propagation angle, are almost similar. The reason is that for this configuration the phase propagation angles of the dominant azimuthal modes $m = \pm 7$ are perpendicular to the stator leading edge angle in any case.

Taking into account the configurations B35V12 and B35V14, the question arises: Why does the mode $m = -1$ carry a lower sound power than the modes $m = \pm 7$? The answer is the influence of both, the phase propagation angle and the cut-on factor. Besides the phase propagation angle of the mode $m = -1$, which is almost congruent to the stator leading edge angle, the cut-on factor is close to 1. Both effects lead to a lower sound power level. A cut-on factor close to 1 is the second aspect why the upstream and downstream BPF1 sound power levels of the configuration with 12 stator vanes are comparable or lower than the sound power levels of adjacent blade counts.

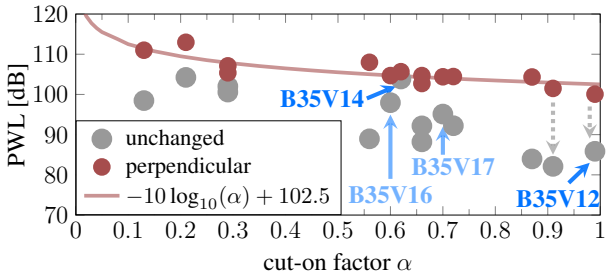

(a) upstream

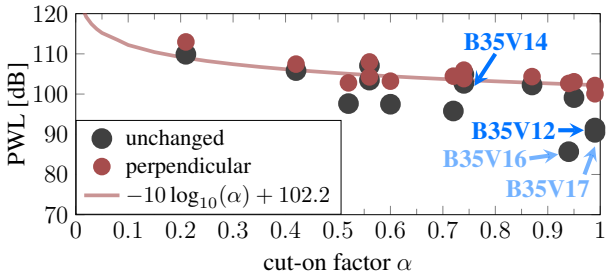

(b) downstream

Figure 6: Upstream and downstream sound power levels of the BPF1 as a function of the cut-on factor α for $B = 35$ and different stator vane counts.

The interim conclusion formulated earlier can now be extended as follows: The sound power levels of the blade count pairings from area "A" are mainly affected by the impact of the phase propagation angle and the cut-on factor. For these configurations, low azimuthal mode orders are dominantly excited, the upstream phase propagation angles of the dominant modes are almost congruent to the stator leading edge angle and the dominant modes are far away from the cut-off limit. These effects cause that the dominant modes are excited weakly and carry a lower sound power. Thus, the two acoustic phenomena reduce the tonal interaction noise.
In area "B", the explanations are still valid and the same two phenomena impact the sound excitation. Compared to area "A", the difference is: The downstream phase propagation angle is congruent to the leading edge angle but the upstream phase propagation angle tends to be oriented almost perpendicular to the leading edge angle. This can exemplarily be seen in Fig. 6 by comparing the upstream and downstream sound power levels of the configuration B35V16. Upstream, the data point is located close to the red line, which means that the phase propagation angle is almost perpendicular to the leading edge angle. Downstream, the cut-on factor of the dominant mode is close to one and the phase propagation angle is rather congruent to the leading edge angle resulting in a lower noise level.

5.2. Inverse cut-off of the blade passing frequency tone

In this subsection we examine the low-count OGV configurations from area "C". For all blade count pairings from area "C" the BPF1 tone is cut-off. Conventionally, a cut-off design is realized with stator vane counts larger than the rotor blade count (by factor 2

or more). However, if the tip Mach number is low enough, a cut-off design can also be achieved with fewer stator vanes than rotor blades. This is called an "inverse cut-off" and corresponds to area "C". Area "C" is a promising design space compared to the conventional cut-off design space since the stator vane count is reduced significantly. Hence, this region has the potential to decrease the stator-generated broadband noise and still benefit from the cut-off of the blade passing frequency tone. Consequently, the question arises why large high-speed fan stages are not designed with inverse cut-off of the first blade passing frequency tone? Typically, for these fan stages, the rotor tip Mach number is close to one, or higher. However, in this section we will show that the inverse cut-off effect is restricted to smaller tip Mach numbers.

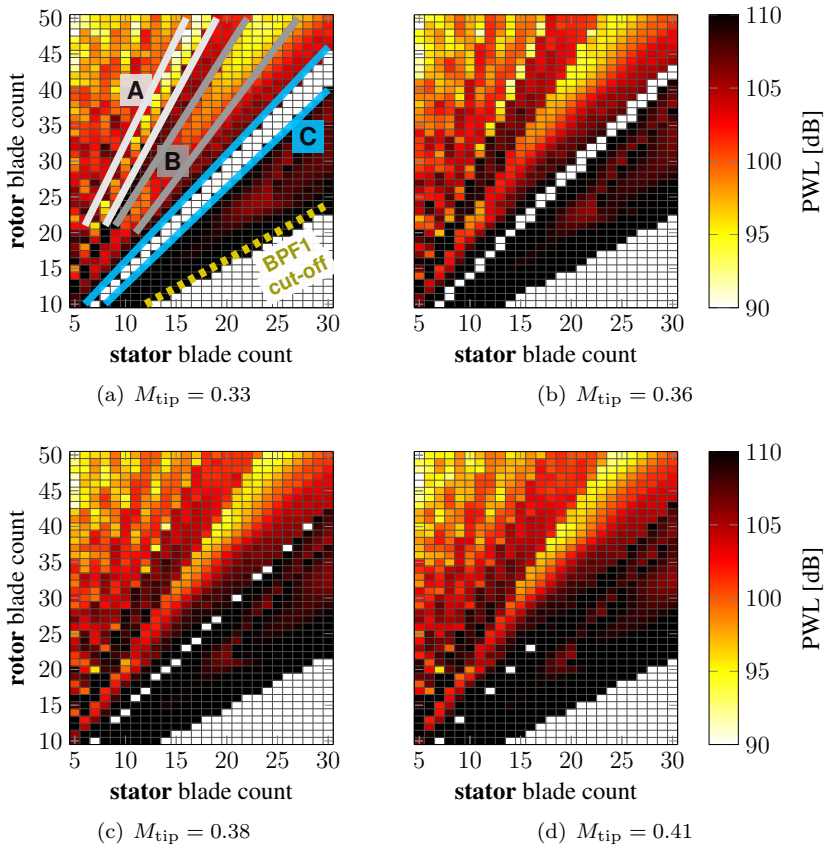

(a) $M_{\text{tip}} = 0.33$ (b) $M_{\text{tip}} = 0.36$

(c) $M_{\text{tip}} = 0.38$ (d) $M_{\text{tip}} = 0.41$

Figure 7: BPF1 sound power levels for different rotor–stator blade count combinations and four rotor tip speeds.

To investigate the formulated question, we analyze the impact of the change of the rotor tip Mach number on the tonal rotor–stator interaction noise. The impact of the tip Mach number is demonstrated by a study on the variation of rotor and stator blade count. This study is performed with the stand-alone module of PropNoise. The fan entry flow Mach number is kept constant at a value of 0.21, which is a typical flight Mach number for small airplanes in cruise condition. In addition, the aerodynamic loading of the rotor and

stator blades is kept constant. As a result, the fan pressure ratio and the fan diameter differ if the tip Mach number changes. In particular, the fan diameter scales inversely with the fan pressure ratio, which means that the lowest rotor tip speed corresponds to the lowest fan pressure ratio and the largest fan diameter. For instance, due to the variation of the rotor tip speed the fan diameter at the rotor tip d_{tip} varies between $d_{tip} = 0.91\,\mathrm{m}$ (for $M_{\mathrm{tip}} = 0.33$) and $d_{tip} = 0.80\,\mathrm{m}$ ($M_{\mathrm{tip}} = 0.41$). The rotor tip Mach number is calculated from $M_{\mathrm{tip}} = (N\, d_{tip}\, \pi)/a$, where N is the rotational speed and a is the speed of sound at the rotor entry.

Figure 7 depicts how the sound power levels of the BPF1 tone vary with the rotor and stator blade counts for four different rotor tip Mach numbers. The tip Mach number 0.33 corresponds to a fan pressure ratio of 1.05 and $M_{\mathrm{tip}} = 0.41$ corresponds to a fan pressure ratio of 1.072. These pressure ratios are realistic for low-speed fan stages of small airplanes.

For all blade count configurations from area "C" the acoustic modes of the BPF1 tone are not able to propagate. The BPF1 tone is cut-off following the inverse cut-off principle. If the rotor tip speed is increased above 0.4, the acoustic modes start to propagate, the blade passing frequency tone becomes cut-on and area "C" shrinks until the effect vanishes completely for larger tip Mach numbers. In other words, the smaller the rotor tip Mach number, the wider the inverse cut-off area, which means that additional blade count pairings become cut-off for lower rotor tip speeds. The variation of the rotor tip Mach number leads to two main observations: First, a correlation between the rotor tip speed and the inverse cut-off effect exists. Second, a decrease of the fan pressure ratio and the rotor tip speed make an inverse cut-off design possible and establish new options in terms of blade count selection within the low-count OGV design space.

Figure 7 indicates that the effect might be restricted to small rotor tip speeds. Additionally, a narrow tip Mach number range exists, below which all blade count pairings from area "C" almost simultaneously become cut-off. Thus, an inverse cut-off design is possible if the rotor tip Mach number is lower than a critical Mach number ($M_{\mathrm{tip}} < M_{\mathrm{tip,\,crit}}$). For cut-off modes, the factor α_{mn} is an imaginary number ($\Re(\alpha) = 0$). Therefore, in absence of swirl, Eq. (2) and $\Re(\alpha) = 0$ lead to the relation

$$M_{\mathrm{tip,\,crit}} = \sqrt{1 - M_x^2}\,\frac{\sigma_{m0}}{B}. \tag{9}$$

Equation (9) shows the correlation between the critical tip Mach number and the inverse cut-off effect. In first approximation, the variable σ_{m0} is equal to $|m|$ in hollow ducts. This simplifies the relation to $M_{\mathrm{tip,\,crit}} \approx \sqrt{1 - M_x^2}\,|m|/B$. As a result, $M_{\mathrm{tip,\,crit}}$ only depends on the axial Mach number M_x and the respective blade count pairing, since the dominant azimuthal mode order m can be expressed as a function of the rotor blade count B and stator vane count V with $m = hB - kV$ (Tyler and Sofrin's rule [29]).

The critical tip Mach number linearly depends on the variable $|m|/B$, which is visualized in Fig. 8(a) for four different axial Mach numbers. The axial Mach number is varied between $M_x = 0.1$ and $M_x = 0.7$ to illustrate the impact of the axial Mach number on $M_{\mathrm{tip,\,crit}}$, although the axial Mach number for the CRAFT rotor–stator stage is $M_x = 0.15$. It can be seen that the impact of M_x on $M_{\mathrm{tip,\,crit}}$ becomes relevant for high axial Mach numbers. In case $M_x < 0.3$, the impact of the axial Mach number is negligible in good approximation. Consequently, the ratio of the triggered mode order and the rotor blade number $|m|/B$ determines the critical tip Mach number in this case. Figure 8(b)

depicts this ratio for all low-count OGV blade count pairings. For each configuration, the lowest possible BPF1 mode order ($|m| = \min(|1 \cdot B - kV|)$) is used to calculate $|m|/B$. To realize an inverse cut-off design for low-speed fan stages, only the blade count pairings from area "C" are suitable. The reason for this is, as shown in Fig. 8(b), that in area "C" an inverse cut-off of the BPF1 tone can be achieved for $M_{\text{tip}} < M_{\text{tip, crit}} \approx |m|/B \approx 0.38$. The fulfillment of this condition may be possible for fan stages with low pressure ratios and large diameters, e.g. fan stages for UAM airplanes. For all other blade count pairings, which do not belong to area "C", the ratio $|m|/B$ is lower than 0.2. That means, M_{tip} would have to be lower than 0.2 to achieve an inverse cut-off. This might not be feasible for a fan design since $M_{\text{tip}} < M_{\text{tip, crit}} = 0.2$ might be too low for the given thrust requirement. Overall, the approximation of $M_{\text{tip, crit}}$ confirms the trend shown in Fig. 7. Regarding the preliminary design of low-speed fan stages, the approximation offers a convenient way to estimate for which blade count pairings an inverse cut-off of the BPF1 tone is possible.

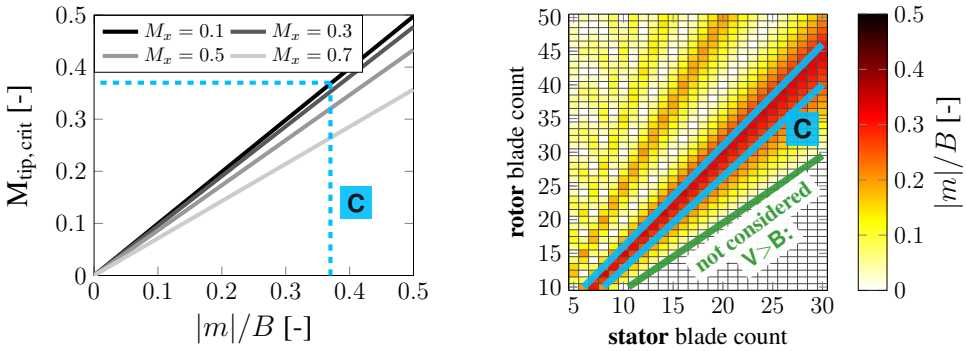

(a) Correlation between $M_{\text{tip, crit}}$ and $|m|/B$

(b) $|m|/B$ for different blade count pairings

Figure 8: Approximation of the critical rotor tip Mach number $M_{\text{tip, crit}}$.

In order to exemplarily verify that the inverse cut-off effect depends on the rotor tip speed, we numerically examined the configuration with 18 rotor blades in combination with 11, 12, 13 and 14 stator vanes. Two different rotor tip speeds are considered, $M_{\text{tip}} = 0.33$ and $M_{\text{tip}} = 0.38$. The analytical prediction from PropNoise is compared with the results obtained from the Harmonic Balance simulation in Tab. 3. For $M_{\text{tip}} = 0.33$ both the analytical and the numerical results predict that the BPF1 modes are not able to propagate if 12 or 13 stator vanes are combined with 18 rotor blades. Thus, the Harmonic Balance simulations confirm that the BPF1 tone is cut-off following the inverse cut-off principle if the rotor tip Mach number is $M_{\text{tip}} = 0.33$. If the tip Mach number is increased to $M_{\text{tip}} = 0.38$, the Harmonic Balance simulations also verify that the acoustic modes start to propagate. Hence, the BPF1 tone becomes cut-on for the higher rotor tip speed. Regarding the configuration with 12 stator vanes, the acoustic mode $(m, n) = (-6, 0)$ becomes cut-on and regarding the configuration with with 13 stator vanes, $(m, n) = (5, 0)$ becomes cut-on.

As a result, an inverse cut-off design can be realized particularly for low-speed fan stages with low fan pressure ratios and large fan diameters (compared to the size of the aircraft). Thus, an inverse cut-off design using the blade count pairings of area "C" may

be promising for fan stages of small airplanes operating in urban areas.

	V11		**V12**		**V13**		**V14**	
	PN	HB	PN	HB	PN	HB	PN	HB
$M_{\text{tip}} = 0.33$	112.0	115.2	inverse cut-off		inverse cut-off		116.0	121.0
$M_{\text{tip}} = 0.38$	112.0	—	113.8	117.3	118.7	123.0	114.8	—

Table 3: BPF1 sound power levels (in [dB]) for 18 rotor blades and varying stator vane count. Comparison between PropNoise and Harmonic Balance simulation for two different rotor tip speeds in order to verify the inverse cut-off effect. Note that "—" indicates that no HB simulation was performed for this configuration.

6. Conclusion and discussion

With the noise assessment presented in this paper, we intended to provide a step towards the design-to-noise of low-speed axial fan stages for small airplanes, which may operate in urban areas. Particularly, we focused on fan stages with fewer stator vanes than rotor blades (low-count OGV fan stages). We illustrated promising mechanisms to reduce the blade passing frequency tone. In summary, our analytical and numerical noise assessment led to the following findings:

- We showed that two acoustic parameters dominantly impact the tonal noise excitation of low-count OGV configurations: The mode phase propagation angle and the mode cut-on factor.
- While varying the rotor and stator blade counts, we identified three low-count OGV design spaces, for which the blade passing frequency tone is either strongly reduced or fully suppressed.
- For two identified low-count OGV design spaces, the phase propagation angle of either the upstream or the downstream dominant mode was congruent to the stator leading edge angle. In that case the acoustic mode is excited weakly and the sound power level is low at noise generation. This mechanism was verified by means of unsteady numerical simulations.
  In addition, for the blade count pairings of those two design spaces, the triggered acoustic interaction modes were far away from the cut-off limit. Hence, these modes propagate well inside the duct segments. However, the results indicated that modes that are further away from the cut-off limit are excited weakly and carry a lower sound power at their generation. Therefore, regarding the noise excitation, we concluded that certain low-count OGV designs acoustically benefit from a combination of both, the impact of the mode phase propagation angle and the impact of the mode cut-on factor.
- For the blade count pairings of the third low-count OGV design space, we observed a cut-off of the blade passing frequency tone even though the number of stator vanes was lower than the number of rotor blades (inverse cut-off). In particular, the variation of the rotor tip speed indicated that decreasing the tip speed makes an inverse cut-off of the blade passing frequency tone possible. The unsteady numerical simulations confirmed the connection between the rotor tip speed and the inverse cut-off effect. Further, our assessment showed that the effect seems to be restricted to small rotor tip speeds. Thus, the inverse cut-off effect could be a

promising tonal noise reduction mechanism for low-speed axial fan stages with low fan pressure ratios.

As a first step towards answering the formulated research question, we focused on the noise excitation and outlined several tonal noise reduction mechanisms for low-count OGV fan stages. The assessment emphasized that specific low-count OGV configurations benefit from a weaker noise excitation, even though the BPF1 tone may be cut-on. Further research should examine the following:

- Although our assessment focused on the first blade passing frequency tone, higher harmonics are also contributing to the fan noise and should be included in subsequent studies.
- Regarding the inverse cut-off effect, the question of the robustness of the cut-off design remains unanswered. In the analytical and the numerical noise prediction an idealized geometry is considered. We assumed that all rotor wakes, which impinge on the stator leading edge, are identical. This is not the case in reality since the rotor blades may vary from another, e.g. due to manufacturing tolerances. Wakes with different width and velocity deficit create new modes that can be cut-on and thus mitigate the inverse cut-off effect.
- We concluded that for certain low-count OGV configurations the resulting interaction modes are far away from the cut-off limit, i.e. these modes propagate efficiently. Therefore, the transmission of sound through the rotor would be an interesting aspect to examine. Philpot [32] states that the blockage of the rotor and the resulting attenuation are larger for acoustic modes that rotate against the rotor rotation.
- Acoustic modes that rotate in the direction of the flow swirl propagate less efficient compared to modes that rotate against the swirl direction [4]. Therefore, for higher swirl Mach numbers, the influence of the flow swirl on the mode propagation would be a further aspect that should be considered to assess the noise reduction potential of low-count OGV designs.
- Another facet of the design-to-noise of fan stages is the noise reduction due to acoustic liner. Regarding the noise propagation, the following question arises: Does an acoustic lining change the observed trends of the blade count variation and can those low-count OGV designs, which benefit from a weaker noise excitation, remain competitive while including the liner damping?

References

[1] W. Neise, L. Enghardt, Technology approach to aero engine noise reduction, Aerosp. Sci. and Technol. 7 (5) (2003) 352–363. doi:10.1016/S1270-9638(03)00027-0.

[2] C. A. Hall, D. Crichton, Engine design studies for a silent aircraft, J. of Turbomach. 129 (3) (2006) 479–487. doi:10.1115/1.2472398.

[3] S. A. Rizzi, D. L. Huff, D. D. Boyd, P. Bent, B. S. Henderson, K. A. Pascioni, D. C. Sargent, D. L. Josephson, M. Marsan, H. He, R. Snider, Urban air mobility noise: Current practice, gaps, and recommendations, NASA/TP-2020-5007433.

[4] R. Jaron, Aeroakustische auslegung von triebwerksfans mittels multidisziplinärer optimierungen, Dissertation, German Aerospace Center, Institute of Propulsion Technology, Berlin, Germany (2018). doi:10.14279/depositonce-7057.

[5] J. H. Dittmar, J. N. Scott, B. R. Leonard, E. G. Stakolich, Effects of long-chord acoustically treated stator vanes on fan noise, NASA Tech. Note, NASA TN D-8062.

[6] J. H. Dittmar, R. P. Woodward, An evaluation of some alternative approaches for reducing fan tone noise, NASA Tech. Memorandum, NASA-TM-105356.
[7] P. J. G. Schwaller, M. J. Oliver, E. Eccleston, Farfield measurements and mode analysis of the effects of vane/blade ratio on fan noise, AIAA/NASA 9th Aeroacoustics Conference, AIAA-84-2280. doi:10.2514/6.1984-2280.
[8] G. Kröger, R. Schnell, N. D. Humphreys, Optimised aerodynamic design of an OGV with reduced blade count for low noise aircraft engines, Proc. of ASME Turbo Expo 2012: Power for Land, Sea and Air, GT2012-69459. doi:10.1115/GT2012-69459.
[9] D. Giacché, T. P. Hynes, S. Baralon, J. Coupland, N. Humphreys, P. Schwaller, Acoustic optimization of ultra-low count bypass outlet guide vanes, 19th AIAA/CEAS Aeroacoustics Conference, AIAA 2013-2295. doi:10.2514/6.2013-2295.
[10] D. Casalino, F. Diozzi, R. Sannino, A. Paonessa, Aircraft noise reduction technologies: A bibliographic review, Aerosp. Sci. and Technol. 12 (1) (2008) 1–17. doi:10.1016/j.ast.2007.10.004.
[11] U. Tapken, L. Caldas, R. Meyer, M. Behn, L. Klähn, R. Jaron, A. Rudolphi, New test facility to investigate the noise generated by shrouded fans for small aircraft applications, DICUAM 2021.
[12] R. Jaron, A. Moreau, Laufschaufeloptimierung der Rotor-Stator-Stufe für den CRAFT-Prüfstand, Tech. Rep. DLR IB 92517-11/B25.
[13] A. Moreau, A unified analytical approach for the acoustic conceptual design of fans for modern aero-engines, Dissertation, German Aerospace Center, Institute of Propulsion Technology, Berlin, Germany (2017). doi:10.14279/depositonce-5935.
[14] E. Rice, M. Heidmann, T. Sofrin, Modal propagation angles in a cylindrical duct with flow and their relation to sound radiation, 17th Aerospace Sciences Meeting, AIAA 79-0183. doi:10.2514/6.1979-183.
[15] A. Moreau, S. Guérin, S. Busse, A method based on the ray structure of acoustic modes for predicting the liner performance in annular ducts with flow, International Conference on Acoustics NAG/DAGA 2009 conference proceedings (2009) 1248–1251.
[16] A. Moreau, S. Guérin, Similarities of the free-field and in-duct formulations in rotor noise problems, 17th AIAA/CEAS Aeroacoustics Conference (32nd AIAA Aeroacoustics Conference), AIAA 2011-2759. doi:10.2514/6.2011-2759.
[17] S. Rienstra, B. Tester, An analytic green's function for a lined circular duct containing uniform mean flow, 11th AIAA/CEAS Aeroacoustics Conference, AIAA 2005-3020. doi:10.2514/6.2005-3020.
[18] S. Guérin, Farfield radiation of induct-cutoff pressure waves, 23rd AIAA/CEAS Aeroacoustics Conference, AIAA 2017-4037. doi:10.2514/6.2017-4037.
[19] W. R. Sears, Some aspects of non-stationary airfoil theory and its practical application, J. of the Aeronautical Sci. 8 (3) (1941) 104–108. doi:10.2514/8.10655.
[20] D. Nürnberger, F. Eulitz, S. Schmitt, A. Zachcial, Recent progress in the numerical simulation of unsteady viscous multistage turbomachinery flow, ISOABE 2001-1081.
[21] H. Yang, D. Nürnberger, H. P. Kersken, Towards excellence in turbomachinery computational fluid dynamics: A hybrid structured-unstructured Reynolds-averaged Navier-Stokes solver, J. of Turbomach. 128(2) (2006) 390–402. doi:10.1115/1.2162182.
[22] K. C. Hall, K. Ekici, J. P. Thomas, E. H. Dowell, Harmonic balance methods applied to computational fluid dynamics problems, Int. J. of Comput. Fluid Dyn. 27 (2) (2013) 52–67. doi:10.1080/10618562.2012.742512.
[23] C. Frey, G. Ashcroft, H. Kersken, C. Voigt, A harmonic balance technique for multistage turbomachinery applications, ASME Turbo Expo 2014: Turbine Technical Conference and Exposition, GT2014-25230. doi:10.1115/GT2014-25230.
[24] D. Wang, X. Huang, A complete rotor–stator coupling method for frequency domain analysis of turbomachinery unsteady flow, Aerosp. Sci. and Technol. 70 (2017) 367–377. doi:10.1016/j.ast.2017.08.025.
[25] F. R. Menter, M. Kuntz, R. Langtry, Ten years of industrial experience with the SST turbulence model, Heat and Mass Transfer 4 (2003) 625–632.
[26] A. Wohlbrandt, C. Weckmüller, S. Guérin, A robust extension to the triple plane pressure mode matching method by filtering convective perturbations, International J. of Aeroacoustics 15(1-2) (2016) 41–58. doi:10.1177/1475472X16630842.
[27] N. C. Ovenden, S. W. Rienstra, Mode-matching strategies in slowly varying engine ducts, AIAA J. 42 (2016) 1832–1840. doi:10.1115/GT2014-25230.
[28] S. Guérin, A. Moreau, U. Tapken, Relation between source models and acoustic duct modes, 15th AIAA/CEAS Aeroacoustics Conference, AIAA 2013-2295. doi:10.2514/6.2009-3364.
[29] J. M. Tyler, T. G. Sofrin, Axial flow compressor noise studies, SAE Internationaldoi:10.4271/

620532.
[30] E. J. Rice, Inlet noise suppressor design method based upon the distribution of acoustic power with mode cutoff ratio, Advances in Eng. Sci. 3 (1976) 883–894.
[31] M. V. Lowson, Theoretical studies of compressor noise, NASA Contractor Rep. NASA CR-1287.
[32] M. G. PHILPOT, The role of rotor blade blockage in the propagation of fan noise interaction tones, AIAA 2nd Aeroacoustics Conference. doi:10.2514/6.1975-447.